CLARIFYING THE IMPLEMENTATION OF WARPING IN THE COMBINED LOCAL GLOBAL METHOD FOR OPTIC FLOW COMPUTATION

Riadh Fezzani, Frédéric Champagnat, Guy Le Besnerais

ONERA/DTIM, www.onera.fr
29 av. Division Leclerc, BP-72, 92322 Châtillon Cedex, FRANCE
{rfezzani,fchamp,lebesner}@onera.fr

ABSTRACT

The field of optical flow techniques in vision is presently dominated by *global* variational techniques based on pixel-wise matching costs, *ie.* based on the Horn & Schunck paradigm, as opposed to *local* window based matching costs, *ie.* based on the Lucas-Kanade paradigm. Motivated by the needs of some difficult real world data we underline the practical interest of the combined local global (CLG) method proposed by Bruhn *et al.* that combines both approaches.

We will show that embedding the basic first order CLG equations in a large displacement iterative framework leads to a technical difficulty. We shall see how Bruhn *et al.* implicitly deal with this difficulty and we will propose an alternative approximation that yields fewer computations and performs equally well.

1. INTRODUCTION

Modern optical flow algorithms find their roots in approaches that appeared in the 80's. We can classify them into local window based methods and global techniques. According to Middlebury rating, the latter generally provides better results

However, global methods are known to be noise sensitive. Combining local and global approaches is the solution given by Bruhn *et al.* [3]. This method has the advantage of supposing some local regularity in addition to the global regularity. This property improves the robustness of the method and makes it a good candidate for real world application sequences with poor image quality, such as sequences from aerial videos from unmanned aerial vehicle (UAV) and Particle Image Velocimetry (PIV).

Figure 2 illustrates well the later context. The studied sequence here is a synthetic set of images generated with the EUROPIV Synthetic Image Generator (SIG) [6] consisting in a series of 30 vortices. We present in figure 1 an image from this sequence and the norm of the ground truth. Figure 2 shows the qualitative differences between the local approach, the global approach and the proposed combined local global method. We see here the contour plot of the norm of the solutions given by these three methods in a close-up on the seventh vortex (starting from the top left). The global method solution looks noisy while the local method gives a smooth but inaccurate solution. The CLG method clearly gives the better result.

Our contribution concerns the large displacement context where the so called optical flow constraint (OFC) is not sufficient. Indeed, in figure 4 the maximum flow reaches 8 pixels. Bruhn *et al.* adopt a classical iterative OFC approach in their original work on CLG. It consists in iteratively rewriting an OFC equation with images warped by the previously estimated flow.

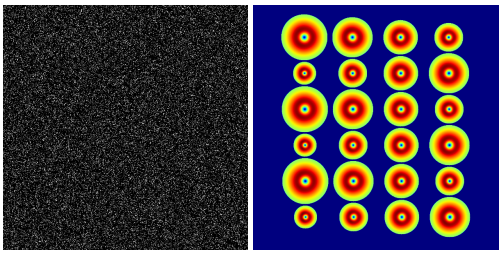

Figure 1: **Left**: Example of a frame from a synthetic PIV sequence representing a grid of vortices with different radius and velocity. **Right**: Norm of the ground truth.

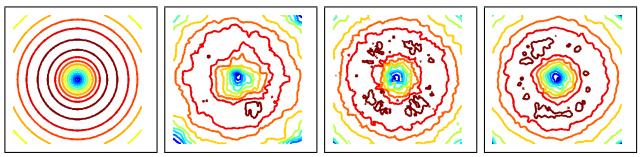

Figure 2: Zoom on the seventh vortex of the PIV sequence of figure 1. **First**: L^2-norm of the ground truth. **Second**: L^2-norm of the local method FOLKI [4] result using a window radius equal to 10 pixels. **Third**: L^2-norm of the TV-L^1 [12] global method result with $\lambda = 40$, $\theta = 0.25$, $\varepsilon = 0.1$ and no edge weighting. **Fourth**: L^2-norm of our CLG implementation result using $\alpha = 60$ and a window radius equal to 3 pixels.

This iterative warping approach has been justified in the global context [8]. However we show that this demonstration does not work in the CLG framework and we explicit the approximation made by Bruhn *et al.*

Starting from the intensity conservation criterion in the large displacement context, we propose a finer approximation which can be considered as an original justification of warping technique in CLG.

The resulting method leads to results very close to CLG actually slightly smoother for identical parameters. It appears well adapted to PIV flow field estimation as shown in our results.

In the next section we recall basic notions concerning local and global estimation in the large displacement context. We then develop the theoretical foundation of warping approach in CLG and elaborate our modified iterative warping scheme (MIWS).

In the fourth section we describe our algorithm which uses a preconditioned block relaxation method that improves the robustness of the solver. Finally we give some experimental results and concluding remarks.

 ISSN 2076-1465

2. BASIS NOTIONS ON OPTICAL FLOW ESTIMATION

Estimation of the optical flow rely on the intensity conservation (IC) assumption:

$$I(\mathbf{x}) = I(\mathbf{x}+\mathbf{u}(\mathbf{x})). \tag{1}$$

Here, $I : \Omega \subset \mathbb{R}^2 \times \mathbb{R} \to \mathbb{R}$ is a rectangular image sequence, $\mathbf{x} \triangleq (x,y,t)$ represents the spatio-temporal coordinates and $\mathbf{u} \triangleq (u,v,1)$ is the unknown optical flow between images at time t and $t+1$.

Loosely speaking, assumption (1) means that the intensity variation of an image in a sequence is mainly explained by motion of intensity patterns.

Many methods start from a first order linearization of (1) around an uniformly null flow, the so-called optical flow constraint (OFC):

$$I_x u + I_y v + I_z = 0 \tag{2}$$

where $I_x \triangleq \frac{\partial I}{\partial x}$, $I_y \triangleq \frac{\partial I}{\partial y}$ and $I_z \triangleq I(\mathbf{x}) - I(\mathbf{x}+\mathbf{u}(\mathbf{x}))$. Using $\nabla_3 I \triangleq (I_x, I_y, I_z)^T$, (2) can be written as $\mathbf{u}^T \nabla_3 I = 0$.

Initially, optical flow methods where based on the OFC, because they assumed small motions between frames. Methods based on the non linear IC criterion (1) have been introduced to deal with the large displacement context [1, 4, 8].

2.1 Local approach

The Lukas-Kanade method [7] assumes constant motion within a window centered at each pixel and deals with square displaced frames difference. According to this, we have to minimize on every $\mathbf{x} \in \Omega$ the least-squares problem:

$$\min_{\mathbf{u}} K_\rho * \left((I(\cdot) - I(\cdot + \mathbf{u}(\mathbf{x})))^2 \right) \tag{3}$$

where K_ρ is a truncated Gaussian window with standard deviation $\rho > 0$. The symbol "$\cdot$" is here the dummy variable for the convolution operation.

We obtain an approximation to (3) using (2):

$$\min_{\mathbf{u}} \mathbf{u}^T [\nabla_3 I \nabla_3^T I]_\rho \mathbf{u} \tag{4}$$

where $[\cdot]_\rho \triangleq K_\rho * (\cdot)$.

2.2 Global linearized approach

Horn and Schunck [5] decided to suppose a global regularity of the flow in Ω. This leads to minimize the global energy functional:

$$\min_{\mathbf{u}} \iint_\Omega \underbrace{\mathbf{u}^T \nabla_3 I \nabla_3^T I \mathbf{u}}_{\textit{data term}} + \underbrace{\alpha(|\nabla u|^2 + |\nabla v|^2)}_{\textit{smoothing term}} dxdy$$

$\alpha \in \mathbb{R}_+$ is a tuning parameter controlling the regularization.

2.3 CLG approach

Combining these two points of view in [3], Bruhn *et al.* proposed to minimize the following global energy functional:

$$\min_{\mathbf{u}} \iint_\Omega \mathbf{u}^T [\nabla_3 I \nabla_3^T I]_\rho \mathbf{u} + \alpha(|\nabla u|^2 + |\nabla v|^2) dxdy \tag{5}$$

Criteria (4) is the integrand in the first term of (5).

Problem (5) is equivalent to the Euler-Lagrange system:

$$\begin{cases} \alpha \Delta u - [I_x^2]_\rho u - [I_x I_y]_\rho v - [I_x I_z]_\rho = 0 \\ \alpha \Delta v - [I_x I_y]_\rho u - [I_y^2]_\rho v - [I_y I_z]_\rho = 0. \end{cases} \tag{6}$$

Bruhn *et al.* , in their implementation, used a stable approximation of the L^1-norm by applying a convex ψ-function to both the regularization and data term.

3. DEALING WITH LARGE DISPLACEMENTS

Note that both HS and Bruhn *et al.* start from a linearized OFC constraint.

3.1 Bruhn *et al.* approach

To handle large displacement, Bruhn *et al.* rely on a so-called iterative warping scheme (IWS), *ie.* they iterate on (5) with I_z replaced by

$$I_z^n \triangleq I(\mathbf{x} + \mathbf{u}_n(\mathbf{x})) - I(\mathbf{x}) \tag{7}$$

where $\mathbf{u}_n$ is the previously estimated flow.

Introducing the motion increment $\delta\mathbf{u}_n \triangleq (\delta u_n, \delta v_n, 0)$ at step n, the sought flow writes:

$$\mathbf{u}_{n+1} = \mathbf{u}_n(\mathbf{x}) + \delta\mathbf{u}_n(\mathbf{x}). \tag{8}$$

The problem at hand is

$$\min_{\delta\mathbf{u}_n} \iint_\Omega \delta\mathbf{u}_n{}^T [\nabla_3 I^n \nabla_3^T I^n]_\rho \delta\mathbf{u}_n + \alpha(|\nabla u_{n+1}|^2 + |\nabla v_{n+1}|^2) dxdy \tag{9}$$

where $I^n(\mathbf{x}) \triangleq I(\mathbf{x} + \mathbf{u}_n(\mathbf{x}))$ and $\nabla_3 I^n \triangleq (I_x^n, I_y^n, I_z^n)^T$. Finally, the derived Euler-Lagrange equations are:

$$\begin{cases} \alpha(\Delta u_n + \Delta\delta u_n) - [(I_x^n)^2]_\rho \delta u_n - [I_x^n I_y^n]_\rho \delta v_n - [I_x^n I_z]_\rho = 0 \\ \alpha(\Delta v_n + \Delta\delta v_n) - [I_x^n I_y^n]_\rho \delta u_n - [(I_y^n)^2]_\rho \delta v_n - [I_y^n I_z]_\rho = 0. \end{cases}$$

3.2 How to justify an IWS approach in CLG ?

Let us consider a large displacement framework from the start by seeking the minimum of the following energy:

$$\min_{\mathbf{u}} \iint_\Omega K_\rho * (I(\cdot) - I(\cdot + \mathbf{u}(\mathbf{x})))^2 + \alpha(|\nabla u|^2 + |\nabla v|^2) dxdy. \tag{10}$$

In 2004, Papenberg [8] showed that minimizing (10) with $\rho = 0$ can be done by an IWS. However, we show in the following that this result does not extend trivially to the case $\rho \neq 0$.

3.3 How to interpret Bruhn *et al.* IWS ?

Can we interpret the Bruhn *et al.* criterion (9) as a first order expansion of (10) using the increment (8)?

Injecting (8) in (10), the integrand of the data term writes:

$$\begin{aligned} & K_\rho * (I(\cdot + \mathbf{u}_{n+1}(\mathbf{x})) - I(\cdot))^2 \\ &= \iint_{\mathbb{R}} K_\rho(\mathbf{x}' - \mathbf{x}) (I(\mathbf{x}' + \mathbf{u}_n(\mathbf{x}) + \delta\mathbf{u}_n(\mathbf{x})) - I(\mathbf{x}'))^2 dx'dy' \\ &\approx \iint_{\mathbb{R}} K_\rho(\mathbf{x} - \mathbf{x}') \big(I(\mathbf{x}' + \mathbf{u}_n(\mathbf{x})) - I(\mathbf{x}') + \\ &\qquad \delta u_n(\mathbf{x}) I_x(\mathbf{x}' + \mathbf{u}_n(\mathbf{x})) + \\ &\qquad \delta v_n(\mathbf{x}) I_y(\mathbf{x}' + \mathbf{u}_n(\mathbf{x})) \big)^2 dx'dy'. \end{aligned} \tag{11}$$

In general, the data term which derives from (11) is not equal to the one of (9).
The difference is that intensity and gradient of the image I are taken at point $\mathbf{x}'+\mathbf{u}_n(\mathbf{x}')$ in (9) while they are taken at $\mathbf{x}'+\mathbf{u}_n(\mathbf{x})$ in (11). Actually they are two cases where (9) and (11) can be identified:

- the case where $\mathbf{u}_n$ is uniformly constant.
- the case where $\rho = 0$, which reduces to the usual global context.

we conclude that the reasoning of Papenberg *et al.* [8] can not be extended to justify Bruhn *et al.* iterative CLG technique.

3.4 A modified IWS

The problem discussed in section 3.3 has been identified in a purely local context in [4]. While the classical IWS linearizes the image intensity $I(\mathbf{x}'+\mathbf{u}_{n+1}(\mathbf{x}))$ around $(\mathbf{x}'+\mathbf{u}_n(\mathbf{x})$ rising (8), we propose a modified IWS based on the linearization of $I(\mathbf{x}'+\mathbf{u}_{n+1}(\mathbf{x}))$ around $(\mathbf{x}'+\mathbf{u}_n(\mathbf{x}'))$.

This way, we expand the data term of the large displacement CLG criterion (10) as:

$$\begin{aligned}
&K_\rho * \left(I(\cdot+\mathbf{u_{n+1}}(\mathbf{x}))-I(\cdot)\right)^2 \\
&= \iint_{\mathbb{R}} K_\rho(\mathbf{x}-\mathbf{x}')\big(I(\mathbf{x}'+\mathbf{u_n}(\mathbf{x}')+\mathbf{u_{n+1}}(\mathbf{x})-\mathbf{u_n}(\mathbf{x}')) \\
&\qquad -I(\mathbf{x}')\big)^2 d\mathbf{x}'d\mathbf{y}' \\
&\approx \iint_{\mathbb{R}} K_\rho(\mathbf{x}-\mathbf{x}')\big(I(\mathbf{x}'+\mathbf{u_n}(\mathbf{x}'))-I(\mathbf{x}')+ \\
&\qquad (u_{n+1}(\mathbf{x})-u_n(x'))I_x(\mathbf{x}'+\mathbf{u_n}(\mathbf{x}'))+ \\
&\qquad (v_{n+1}(\mathbf{x})-v_n(x'))I_y(\mathbf{x}'+\mathbf{u_n}(\mathbf{x}'))\big)^2 d\mathbf{x}'d\mathbf{y}' \\
&= K_\rho * \left((\mathbf{u}_{n+1}(\mathbf{x})^T\bar{\nabla}_3 I^n(\cdot))^2\right) \\
&= {\mathbf{u}_{n+1}}^T[\bar{\nabla}_3 I^n \bar{\nabla}_3^T I^n]_\rho \mathbf{u}_{n+1}, \qquad (12)
\end{aligned}$$

where we defined

$$\begin{aligned}
\bar{I}_z^n &\triangleq I^n(\mathbf{x})-I(\mathbf{x})-u_n I_x^n(\mathbf{x})-v_n I_y^n(\mathbf{x}). \qquad (13)\\
\bar{\nabla}_3 I^n &\triangleq (I_x^n, I_y^n, \bar{I}_z^n)^T.
\end{aligned}$$

At each step n of the proposed MIWS approach we optimize the criterion:

$$\min_{\mathbf{u}_{n+1}} \iint_\Omega {\mathbf{u}_{n+1}}^T[\bar{\nabla}_3 I^n \bar{\nabla}_3^T I^n]_\rho \mathbf{u}_{n+1} + \alpha(|\nabla u_{n+1}|^2+|\nabla v_{n+1}|^2)dxdy. \qquad (14)$$

This criterion is very similar to (9), the differences being in the computation of $\bar{I}_z^n$ (13) which includes additional terms with regards to (7) and that minimizing the quadratic form (14) gives the total flow field $\mathbf{u}_{n+1}$ rather the increment $\delta\mathbf{u}_n$ as (9).

The corresponding Euler-Lagrange equations are similar to (6):

$$\begin{cases} \alpha\Delta u_{n+1} - [(I_x^n)^2]_\rho u_{n+1} - [I_x^n I_y^n]_\rho v_{n+1} - [I_x^n \bar{I}_z]_\rho = 0 \\ \alpha\Delta v_{n+1} - [I_x^n I_y^n]_\rho u_{n+1} - [(I_y^n)^2]_\rho v_{n+1} - [I_y^n \bar{I}_z]_\rho = 0. \end{cases}$$

4. ROBUST NORM

For the sake of simplicity and for shorthand writing, we described previously our approach using the L^2-norm, but we choose in our implementation to approximate the L^1-norm as in [8]. In fact, used in the data term, the L^1-norm ensure robustness in occlusion regions, and in the regularization term, it allow regularization while preserving the flow discontinuities. So we apply $\psi(|x|^2)=\sqrt{|x|^2+\varepsilon}\approx|x|$ to both data and regularization term (where $\varepsilon=10^{-6}$ ensure the differentiability of ψ in 0).

This way, the Euler-Lagrange equations for CIWS become:

$$\begin{aligned}
0 &= \psi_D\cdot\left([(I_x^n)^2]_\rho\delta u_n + [I_x^n I_y^n]_\rho\delta v_n + [I_x^n I_z^n]_\rho\right) \\
&\quad -\alpha\cdot\mathtt{div}(\psi_R\cdot\nabla u_{n+1}) \\
0 &= \psi_D\cdot\left([(I_y^n)^2]_\rho\delta v_n + [I_x^n I_y^n]_\rho\delta u_n + [I_y^n I_z^n]_\rho\right) \\
&\quad -\alpha\cdot\mathtt{div}(\psi_R\cdot\nabla v_{n+1}) \qquad (15)
\end{aligned}$$

where

$$\begin{aligned}
\psi_D &\triangleq \psi'(\delta\mathbf{u}_n{}^T[\nabla_3 I^n\nabla_3^T I^n]_\rho\delta\mathbf{u}_n) \\
\psi_R &\triangleq \psi'(|\nabla u_{n+1}|^2+|\nabla v_{n+1}|^2).
\end{aligned}$$

To obtain the Euler-Lagrange equations corresponding to MIWS, we just need to replace respectively $(\delta\mathbf{u}_n, I_z^n, \nabla_3 I^n)$ by $(\mathbf{u}_{n+1}, \bar{I}_z^n, \bar{\nabla}_3 I^n)$ in (15):

$$\begin{aligned}
0 &= \psi_D\cdot\left([(I_x^n)^2]_\rho u_{n+1} + [I_x^n I_y^n]_\rho v_{n+1} + [I_x^n \bar{I}_z^n]_\rho\right) \\
&\quad -\alpha\cdot\mathtt{div}(\psi_R\cdot\nabla u_{n+1}) \\
0 &= \psi_D\cdot\left([(I_y^n)^2]_\rho v_{n+1} + [I_x^n I_y^n]_\rho u_{n+1} + [I_y^n \bar{I}_z^n]_\rho\right) \\
&\quad -\alpha\cdot\mathtt{div}(\psi_R\cdot\nabla v_{n+1}). \qquad (16)
\end{aligned}$$

5. IMPLEMENTATION DETAILS

To make some comparisons between CIWS and MIWS, we wrote a python code [9] using the weave[1] package to embed C++ code and accelerate some critical part of the program. We will now describe the algorithm that we designed.

We discretize the equations (15) and (16) using finite difference schemes: image derivatives I_x and I_y are approximated at the third order and the flow derivatives (in ψ_R) at the second order.

We then implemented a 2×2 block SOR solver [10] also known as coupled point solver [2]. To this end, we ordered our linear system to put the 2×2 blocks corresponding to (15) for each pixel on the diagonal and we solved them using Cramer's method. This allows us to update a flow vector (u,v) per SOR loop step instead of updating u or v one at a time.
The CIWS Euler-Lagrange equation (15) (respectively the MIWS one (16)) is still non-linear due to the terms with the ψ function. We fix that by using an implicit scheme *ie.* by freezing ψ_D with $\delta\mathbf{u}_{n-1}$ (respectively $\mathbf{u}_n$) and ψ_R with the previous SOR iterate of $\delta\mathbf{u}_n$ (respectively $\mathbf{u}_{n+1}$).

5.1 Preconditioned SOR solver

During our experiments, it appeared that some of the 2×2 systems that we solve in the loop of our smoother may have a very large condition number. This makes the result of these

[1] http://www.scipy.org/Weave

local systems erroneous and may affect the convergence and the quality of the global solution. To address this, we choose to apply the Jacobi preconditioner [10] that simply consists in taking the diagonal of the matrix as preconditioner. Finally, rather then solving

$$\begin{pmatrix} a & b \\ b & c \end{pmatrix} \begin{pmatrix} u \\ v \end{pmatrix} = \begin{pmatrix} e \\ f \end{pmatrix}$$

we solve the equivalent system

$$\begin{pmatrix} a^{-1} & 0 \\ 0 & c^{-1} \end{pmatrix} \begin{pmatrix} a & b \\ b & c \end{pmatrix} \begin{pmatrix} u \\ v \end{pmatrix} = \begin{pmatrix} a^{-1} & 0 \\ 0 & c^{-1} \end{pmatrix} \begin{pmatrix} e \\ f \end{pmatrix}$$

which has a smaller condition number.

We embed our preconditioned block-SOR solver in a multilevel scheme performed on a non-dyadic image pyramid with a reduction factor of 0.8 obtained using bilinear interpolation. The image's warping was also made by bilinear interpolation and extrapolation.

5.2 Algorithmic differences between CIWS and MIWS

Algorithm 1 describes the Iterative Warping Scheme. There are three differences between CIWS and MIWS implementations:

(i) The linear systems creation (line 5) is performed according to the corresponding Euler-Lagrange equations: (15) for CIWS and (16) for MIWS,

(ii) care has to be taken with the regularization term in CIWS. In fact, $\mathbf{u}_{n+1} = \mathbf{u}_n + \delta\mathbf{u}_n$ appear in the divergence part of (15), so we have to freeze ψ_R with the last SOR iterate of $\delta\mathbf{u}_n$ and to separate the gradient of $\mathbf{u}_{n+1}$ into known and unknown part,

(iii) in CIWS we need to add $\delta\mathbf{u}_n$ to $\mathbf{u}_n$ to obtain $\mathbf{u}_{n+1}$ after each solving step (line 6).

Algorithm 1 Iterative Warping Scheme

```
1:  Starting from a given initial flow u_n = u_0
2:  for all levels (starting from the coarsest) do
3:      repeat
4:          Warp the image with u_n → I^n
5:          Create the linear system
6:          Solve it using block-SOR→ u_{n+1}
7:      until the number of needed update at each level is
    reached
8:      if current level ≠ finest level then
9:          Prolongate u_{n+1} to the next level
10:     end if
11: end for
```

5.3 Complexity operation comparison

MIWS saves computational time compared with CIWS. In fact, for an $m \times n$ image sequence:

- MIWS needs $4mn$ arithmetic operations more than CIWS per warp due to $\bar{I}_z^n$ computation (13)
- CIWS needs $5mn$ additional arithmetic operations per preconditioned block SOR iteration compared to MIWS, due to the management of the regularization term (ii) and the update of $\mathbf{u}_n$ after each $\delta\mathbf{u}_n$ computation (iii).

Table 1: Comparison of the CIWS and MIWS algorithms regarding the measured average angular error (in degrees) and average endpoint error (in pixels). **Parameters**: $\alpha = 20$ and window radius = 2 pixels.

	Angular Error		Endpoint Error	
	CIWS	MIWS	CIWS	MIWS
Dimetrodon	2.42	**2.36**	0.13	**0.12**
Grove2	2.69	**2.66**	0.19	0.19
Grove3	**6.47**	6.62	**0.67**	0.71
Hydrangea	2.24	**2.23**	**0.18**	0.19
RubberWhale	**4.46**	4.55	0.14	0.14
Urban2	3.02	**2.99**	0.39	0.39
Urban3	**6.79**	7.30	**0.74**	0.80
Venus	**4.67**	4.88	0.31	0.31

Table 2: Comparison of the local and global methods with our two implementation of CLG method (CIWS and MIWS) on the synthetic PIV sequence presented in figure 1. **Parameters**: $\alpha = 60$ and window radius = 3 pixels.

	Local	Global	CIWS	MIWS
Angular error	5.31	4.03	2.93	**2.91**
Endpoint error	0.28	0.17	**0.15**	0.16

Let us say that we perform N_{iter} SOR iteration and N_{warp} warp in our implementation, so we save $mnN_{warp}(5N_{warp} - 4)$ arithmetic operations.

Knowing that in practice N_{iter} may be large, the saved computational time becomes non negligible: In a typical run, MIWS is 12% faster than CIWS.

6. EXPERIMENTAL RESULTS

In order to validate the new iterative algorithm MIWS, we first tested the two algorithms on the frames 10 and 11 of the well known Middlebury's public data set[2] using the same fixed parameter $\alpha = 20$ and a Gaussian convolution window of radius 2.

Knowing the ground truth flow $\mathbf{u_{GT}} = (u_{\mathbf{GT}}, v_{\mathbf{GT}}, 1)$, we measured the endpoint error using the formula $EPE(\mathbf{u}) = \sqrt{(u - u_{\mathbf{GT}})^2 + (v - v_{\mathbf{GT}})^2}$, and the angular error according to $AE(\mathbf{u}) = \arccos\left(\dfrac{\mathbf{u_{GT}} \cdot \mathbf{u}^T}{\|\mathbf{u}\| \cdot \|\mathbf{u_{GT}}\|}\right)$.

We present in table 1 the obtained average errors on the solution given by our CIWS and MIWS algorithms. We obtain essentially the same performances with CIWS and MIWS. Actually, with the same parameters, MIWS leads to slightly smoother results than CIWS. this explains the better performances on Urban3 which is an example with large motion discontinuities.

We also present in table 2 the measured average errors on the solutions obtained on the synthetic PIV sequence presented in figure 1. As expected looking at figure 2, CLG methods gives the best measured results with almost no difference between our two implementations CIWS and MIWS.

Figure 3 is a study of the case 'A' [11] from the PIV challenge [3] 2001 which is a set of experimental images represent-

[2] http://vision.middlebury.edu/flow/data/

[3] http://www.pivchallenge.org/

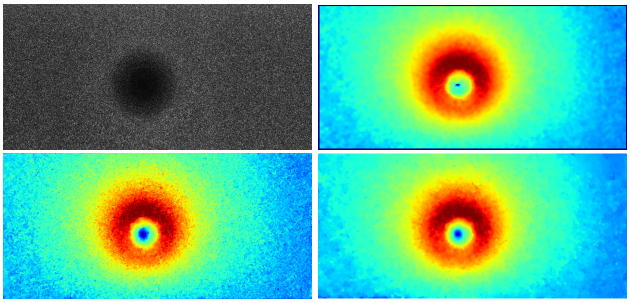

Figure 3: **Top left**: A PIV image from the sequence "A" of the PIV challenge 2001 [11]. **Top right**: L^2-norm of FOLKI [4] result using a window radius equal to 7 pixels. **Bottom left**: L^2-norm of TV-L^1 [12] result with $\lambda = 40$, $\theta = 0.25$, $\varepsilon = 0.1$ and no edge weighting. **Bottom right**: L^2-norm of MIWS result using $\alpha = 60$ and a convlution window with radius equal to 3 pixels.

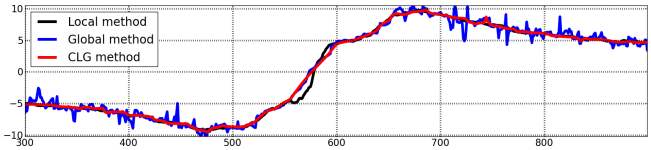

Figure 4: Comparison of a cut along the horizontal line passing through the vortex core of the results presented figure 3.

ing a strong vortex. We present an image from this sequence and the norm of the flows obtained using the FOLKI local method [4], the TV-L^1 global method [12] and the proposed combined local global method MIWS. We also present in figure 4 three curves representing a cut of the vertical component of the estimated flow fields along the horizontal axes passing through the vortex core. The PIV images presents a highly pitched texture that penalizes pixelwise matching cost methods. In fact, the TV-L^1 solution exhibits a strong residual noise clearly observable in the region far from the core. While the local and CLG methods have a satisfactory behavior regarding the noise, they differ noticeably in the core region. In this region the flow gradient is strong and the SNR is low due to the lack of particles (see figure 3): CLG leads to a smoother solution which is physically sound. The CLG method appears here as a good compromise.

Regarding our experiments, we can say that CIWS and MIWS provide equivalent results. We also observed that MIWS gives smoother solutions than CIWS. This is certainly due to its formulation (12) that better modelizes window warping than the original one (9).

Acknowledgment: We thank Benjamin Leclaire from the Department of Fundamental and Experimental Aerodynamics of ONERA (French Aerospace Lab) for providing us with the synthetic PIV sequence and for his valuable comments on our experimental results on PIV images.

7. CONCLUSION

This paper proposed to give some clarifications of the implementation of warping in the combined local global method. In fact, considering the large displacement framework, we identified a shortcoming arising while embedding the CLG method in an iterative warping scheme. We then designed a theoretically justified formulation, and showed a computational time improvement. We presented some experimental results and observed that the two implementations give equivalent results.

We also proposed the use of CLG on the hard real world application PIV and showed its advantages in this field. We believe that combining local and global approach is a good way to address PIV problem.

This work targeted the data part of the CLG method, we plan now to study the regularization part of the optical flow problem looking for a formulation better suited for PIV problem.

REFERENCES

[1] M. J. Black and P. Anandan. Robust dynamic motion estimation over time. In *IEEE computer society conference on computer vision and patern recognition*, pages 296–302, 1991.

[2] A. Bruhn, J. Weickert, C. Feddern, T. Kohlberger, and C. Schnorr. Variational optical flow computation in real time. *IEEE Transactions on Image Processing*, 14(5):608–615, 2005.

[3] A. Bruhn, J. Weickert, and C. Schnörr. Lucas/kanade meets horn/schunck: Combining local and global optic flow methods. *International Journal of Computer Vision*, 61:211–231, 2005.

[4] G. Le Besnerais and F. Champagnat. Dense optical flow by iterative local window registration. In *IEEE International Conference on Image Processing*, 2005.

[5] B. K. P. Horn and B. G. Schunck. Determining optical flow. *Artificial intelligence*, 17:185–203, 1981.

[6] B. Lecordier and J. Westerweel. The EUROPIV synthetic image generator (SIG). In *Particle image velocimetry: recent improvements. Proceedings of the EUROPIV*, volume 2, 2004.

[7] B. D. Lucas and T. Kanade. An iterative image registration technique with an application to stereo vision. In *Seventh international joint conference on artificial intelligence*, pages 674–679, 1981.

[8] N. Papenberg, A. Bruhn, T. Brox, S. Didas, and J. Weickert. Highly accurate optic flow computation with theoretically justified warping. *International Journal of Computer Vision*, 67(2):141–158, 2006.

[9] M. Pilgrim. *Dive into Python*. Apress, 2004.

[10] Y. Saad. *Iterative methods for sparse linear systems*. Society for Industrial Mathematics, 2003.

[11] M. Stanislas, K. Okamoto, and C. Kahler. Main results of the first international PIV challenge. *Measurement Science and Technology*, 14(10):63–89, 2003.

[12] C. Zach, T. Pock, and H. Bischof. A duality based approach for realtime tv-l1 optical flow. In *Pattern Recognition (Proc. DAGM)*, pages 214–223, Heidelberg, Germany, 2007.